Ceramics-Silikáty 67 (2), 189-197 (2023)
www.ceramics-silikaty.cz doi: 10.13168/cs.2023.0017

EFFECT OF ULTRAFINE SLAG POWDER ON THE RHEOLOGICAL BEHAVIOUR, COMPRESSIVE STRENGTH, AND MICROSTRUCTURE OF ULTRA-HIGH PERFORMANCE CONCRETE

CONGQI LUAN*, ZIPENG HAN**, YUONGBO HUANG*, PENG DU*, #ZONGHUI ZHOU*, JINBANG WANG*

*Shandong Provincial Key Laboratory of Preparation and Measurement of Building Materials, University of Jinan, Jinan 250022, China
**School of materials science and engineering, University of Jinan, Jinan 250022, China

#E-mail: mse_zhouzh@ujn.edu.cn

Submitted February 18, 2023; accepted April 4, 2023

Keywords: Ultra-High Performance Concrete, Ultrafine slag powder, Rheology, Pore structure, Microstructure

The effect of the addition of ultrafine slag powder (USL) on the rheology, strength, and porosity of Ultra-High Performance Concrete (UHPC) was investigated, whose microstructure was analysed by XRD, NMR, XPS, and SEM. The results show that whether the USL was incorporated or not, the paste keeps its original shear thickening behaviour. However, the yield stress first increased and then decreased with the addition of the USL content. The change in the compressive strength of the UHPC kept close to that of the yield stress. Incorporating 20 % USL, the UHPC reached a maximum compressive strength of 147.8 MPa, which was increased by 12.2 % compared to the reference sample, and its porosity was 6.72 %, which was decreased by 14% compared to the reference sample. In addition to the formation of more C–S–H gels, the pozzolanic reaction of USL increased the chain length of C-S-H and the binding energy of Ca2p, Si2p, O1s, and Al2p. Furthermore, it reduced the Al/Si ratio and Ca2P-Si2P value, making the paste microstructure more compact.

INTRODUCTION

Ultra-High Performance Concrete (UHPC) has been widely studied for its high strength, durability, and toughness [1]. However, the absence of coarse-size aggregates and a low water-cement ratio increase the cement content compared to ordinary concrete. Using cement on a large scale leads to severe environmental problems in terms of energy and material consumption, greenhouse gas emissions, and an increase in the cost of UHPC [2]. To achieve a low carbon footprint and cost reduction, supplementary cementitious materials (SCMs), such as fly ash, mineral powders, and limestone powders, have gradually started to replace cement and become an integral part of concrete [2-4]. SCMs effectively improve the workability and bulk stability of concrete and enhance the durability of concrete, such as the impermeability and frost resistance.

Slag powder is one of the most suitable SCMs for High-Performance Concretes to replace cement and enhance its mechanical properties [5]. The reactivity of SCMs in cement systems depends not only on the chemical composition, but also on their fineness [6, 7]. The finer the slag particles, the more rounded they are, which significantly improves the workability of fresh concrete and the uniformity of the microstructure at a later stage. [8]. The drying and grinding of slag during processing increases the bonding breakpoints of silicon oxide and alumina and improves the activity of the ultrafine-slag powder (USL) [9]. Therefore, it is interesting to investigate the effect of USL on the hydration of cement. G. Dhinakaran [10] reported that the replacement of cement with USL resulted in a concrete with a higher early strength, lower permeability, and better resistance to chloride ion penetration.

Zengqi Zhang et al. [11] compared the effect of the 20 % substitution of USL and silica fume on cement paste with a low water ratio. The results showed that USL plays a similar effect as that of silica fume, accelerating the hydration, improving the interface transition zone and reducing the porosity of concrete. However, they focused more on USL in maintaining the performance of the concrete based on better cost reduction, while the mechanism of its role was not analysed deep enough. Wang Qianget et al. [6] studied the initial setting time and workability of a cement paste containing USL, and the results showed that the induction period and the initial setting time gradually decreased with an increase in the amount of USL. With the same USL content, the induction period and the initial setting time of the paste shortened with an increase in the particle fineness. To date, the strengths, interfacial transition zone, permeability, and total pore structure of concrete have been shown to be improved by USL [12-15].

Table 1. Chemical composition of the cement and USL (wt. %).

	Na_2O	MgO	Al_2O_3	SiO_2	P_2O_5	SO_3	Cl^-	K_2O	CaO	TiO_2	MnO	Fe_2O_3	LOI
USL	0.66	9.37	16.82	27.39	0	2.60	0.07	0.32	36.31	0.91	0.37	0.33	1.20
Cement	0.50	4.94	8.06	22.89	0.10	3.55	0.11	0.73	52.84	0.38	0.13	2.39	3.27

However, there are few reports on the effect of USL on the rheology and the mechanism of UHPC hydration. Herein, this paper investigates the rheology, strength, and microstructure of UHPC containing USL as well as its interaction mechanism with cement, to lay a foundation for the application of USL in UHPC.

EXPERIMNETAL

Materials

P·O 52.5 ordinary Portland cement was used in this study. The USL was purchased from the market and ground to a fine powder. The chemical composition and particle size distribution of the cement and USL are shown both in Table 1 and Figure 1. A polycarboxylate superplasticiser (Sp) and straight steel fibres were used in this study. The quartz sand was considered as the aggregate. The formulation of the mixtures is shown in Table 2.

Table 2. Mixture proportions of the UHPC ($kg \cdot m^{-3}$).

	P·O 52.5	USL	Water	SP	Sand	Steel fibres
Ref	1150	0	207	17.25	1150	152
USL5	1092.5	57.5	207	17.25	1150	152
USL10	1035	115	207	17.25	1150	152
USL15	977.5	172.5	207	17.25	1150	152
USL20	920	230	207	17.25	1150	152
USL25	862.5	287.5	207	17.25	1150	152
USL30	805	345	207	17.25	1150	152

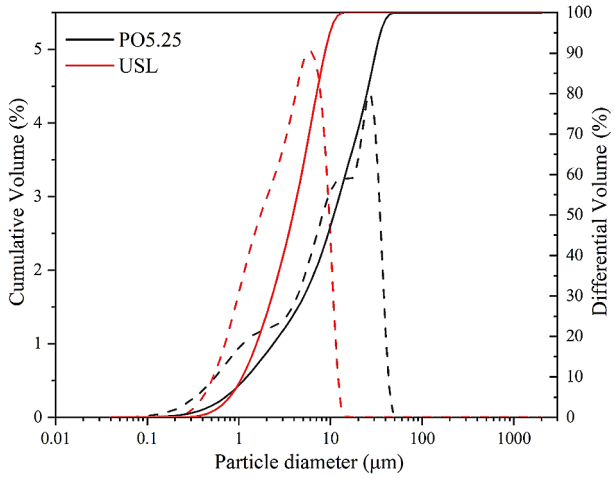

Figure 1. Particle size distribution of the cement and USL.

Methods

A Malvern rheometer and the shear-rate-control protocol are shown in Figure 2. To eliminate the thixotropy, the slurry was pre-sheared for 30 s and then experienced the stepped falling stages, which lasted for 150 s. The results of the compressive strength of the mortar were obtained from six specimens with a loading rate of 2.4 $kN \cdot s^{-1}$. The fragment of the paste was ground into a powder for the X-Ray Diffraction (XRD), X-ray Photoelectron Spectroscopy (XPS), and ^{29}Si NMR (nuclear magnetic resonance) spectroscopy on the designated test day. After passing through a 200-mesh sieve, the powder was heated and dried to a constant weight at 60 °C in a vacuum drying oven.

The powder was pressed into thin sheets for the XRD test and performed at 0.2 s per step from 5° to 60° with CuKα radiation at 40 kV and 40 mA. Scanning electron microscopy (SEM) and backscattered electron (BSE) imaging were used to observe the microstructure of the paste containing USL or LS. Mercury intrusion porosimetry (MIP) was used to evaluate the pore structure of the paste. The solid-state ^{29}Si NMR spectra were obtained from an AVANCE III HD 600 MHz NMR spectrometer with 9.4 T and 79.4 MHz in the magnetic field intensity and magnetic field frequency, respectively.

RESULTS AND DISCUSSION

Rheological behaviour

The rheological curves of the paste with the different USL content are shown in Figure 2. For the reference paste (Ref), the shear stress decreased rapidly with an increasing shear rate, thus belonging to swelling flow

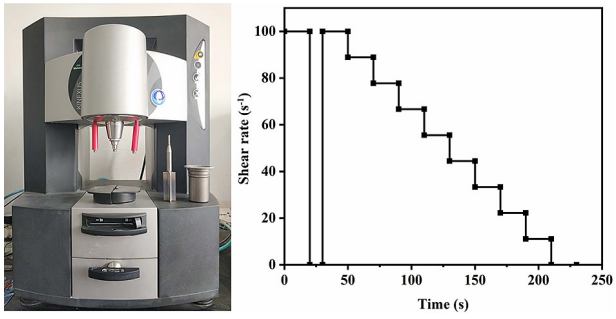

a) b)

Figure 2. Malvern rheometer (a) and Rheological test protocol (b).

type fluids [11]. Incorporating the USL, the fluid type was unchanged, and the non-linear Herschel-Bulkley (Equation 1) model can be used to fit the non-linear flow relationship between the shear stress and the shear rate. The equation is:

$$\tau = \tau_0 + k\gamma^n \quad (1)$$

where τ_0 denotes the yield stress, k denotes the consistency index, and n denotes the index of the rheological behaviour of the slurry.

When $n > 1$, the paste is a swelling fluid of the shear-thickened type [16]. After fitting the rheological curves of the paste, it can be found that the n values of all the groups were greater than 1, which are consistent with the rheological properties of shear thickening. The n-value increased with the amount of USL and then gradually decreased. Similarly, the yield stress of the paste also showed a similar pattern. Because the average particle size of the ultrafine mineral powder was smaller than that of the cement particles, the addition of USL improved the distribution of the cement particles. The fine USL particles filled the particle space and incremented the free water content, which changed the disordered arrangement of the particles and influenced the degree of shear thickening. Furthermore, the large surface area of the USL affected the adsorption of the water reducing agent and its agglomeration effect on the yield stress and rheological index n of the slurry.

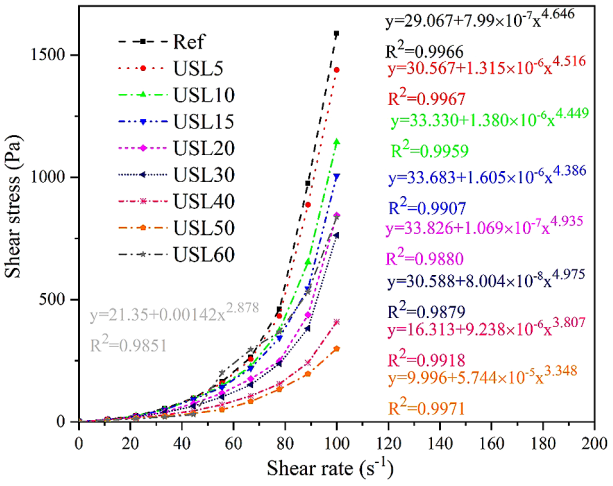

Figure 3. Rheology curves of the cement slurry with the different USL dosages.

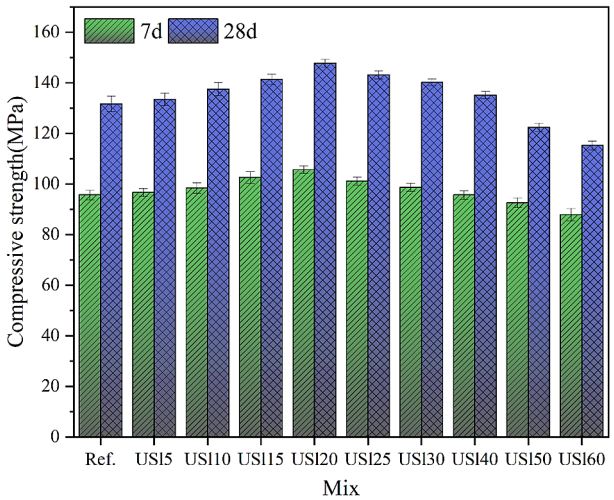

Figure 4. Effect of the USL content on the compressive strength of the UHPC.

reached 147.8 MPa, an increase of 12.2 % compared to the reference sample. This is due to the average particle size of the USL was smaller than that of the cement particles, which filled the pores of the cement particles, leading to a reduction in the porosity and an increase in the compressive strength of the UHPC due to its filling effect [6, 17]. In addition, the USL particles occupied the space that the water initially was encapsulated by the cement particles. The released water prompted the hydration of the cement and improved the compactness of the slurry. Another reason for USL20 obtaining the highest compressive strength at 28 d was that the low water-cement ratio provided a high alkaline environment to stimulate the alkali-activation reactions of the ultrafine slag powder and to produce additional C–S–H gels, increasing the compactness of the cement slurry [18]. The reason for the gradual decrease in the compressive strength of the UHPC when its admixture exceeds 20 % was that the decreasing amount of cement reduced the amount of calcium hydroxide produced by the hydration, while the dilution effect of ultrafine mineral powder on the cement increased, weakening the excitation of USL and reducing the compressive strength of the UHPC. The 28-day compressive strength was 122.5 MPa when the dosage of USL was 50 %, while it was 115.3 MP with 60 % USL, indicating that the UHPC strength did not achieve the requirement of being greater than 120 MPa when the USL content was higher than 50 %.

Compressive strength

The effect of the USL content on the compressive strength of the UHPC is shown in Figure 4. The compressive strength of the UHPC showed a tendency to increase and then decrease with an increase in the admixture of USL at all the curing ages. The 28-d compressive strength of the UHPC containing 20 % USL

XRD analysis

Figure 5 shows the XRD spectra of the cement paste at 1 day and 28 days with the different USL content. The hydration products of $Ca(OH)_2$, ettringite, and monocarboaluminate, together with the unreacted C_3S and C_2S minerals were observed [19]. When incorporating USL in the cement, the hydration product

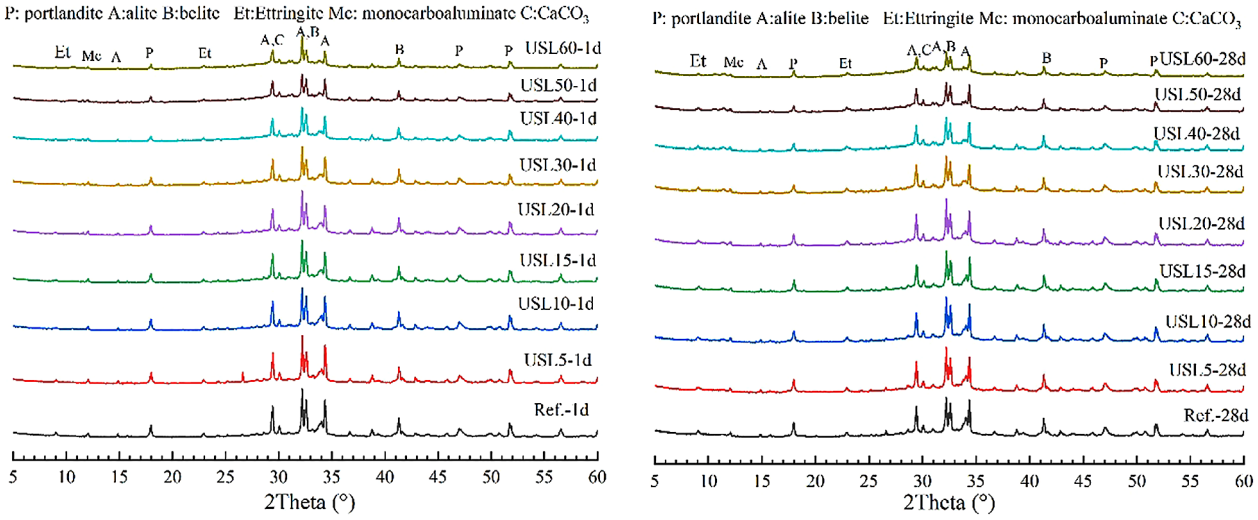

a) 1 day b) 28 days

Figure 5. XRD patterns of the cement paste with the different USL content at 1 day and 28 days.

species in the paste was unchanged and no new phases were observed, but the intensity of the diffraction peaks of $Ca(OH)_2$ was affected. Comparing the $Ca(OH)_2$ characteristic peaks around 2θ = 18° and 34°, it can be seen that the intensity of the $Ca(OH)_2$ characteristic peaks of the same age in the paste containing USL was lower than that of in the Ref. This indicated a significant effect of the USL on the reduction of the $Ca(OH)_2$ content in the cement pastes. There are two reasons for this phenomenon: firstly, the replacement of cement by USL in the mass reduced the amount of water hydration, which decreased the $Ca(OH)_2$ production; secondly, USL has favourable conditions to exploit its pozzolanic reaction in a high alkali environment, which consumed a large amount of $Ca(OH)_2$. The combined effect of both decreased the $Ca(OH)_2$ content of the paste.

^{29}Si NMR

The main hydration products in the paste were C–S–H gels in addition to $Ca(OH)_2$. However, due to the poor crystallinity of the C–S–H gel, it was not easily revealed on the XRD pattern. The C–S–H gel polymerisation was further analysed using ^{29}Si NMR and the results are shown in Figure 6 and Table 3. The clinker (C_3S+C_2S) signals at –70.8 ppm and –71.0 ppm corresponded to Q^0 in the Ref and USL20, respectively [19]. Due to the hydration and pozzolanic reaction of the USL, the relative intensity of Q^0 in USL20 was lower than that of the Ref at 28 d, hence, the signal position of Q^0 in USL20 shifted to the left. Furthermore, the phase left of Q^2(1Al), representing the C–S–H chain end (Q^1), the bridging Q^2(1Al), and the paired site Q^2(0Al)

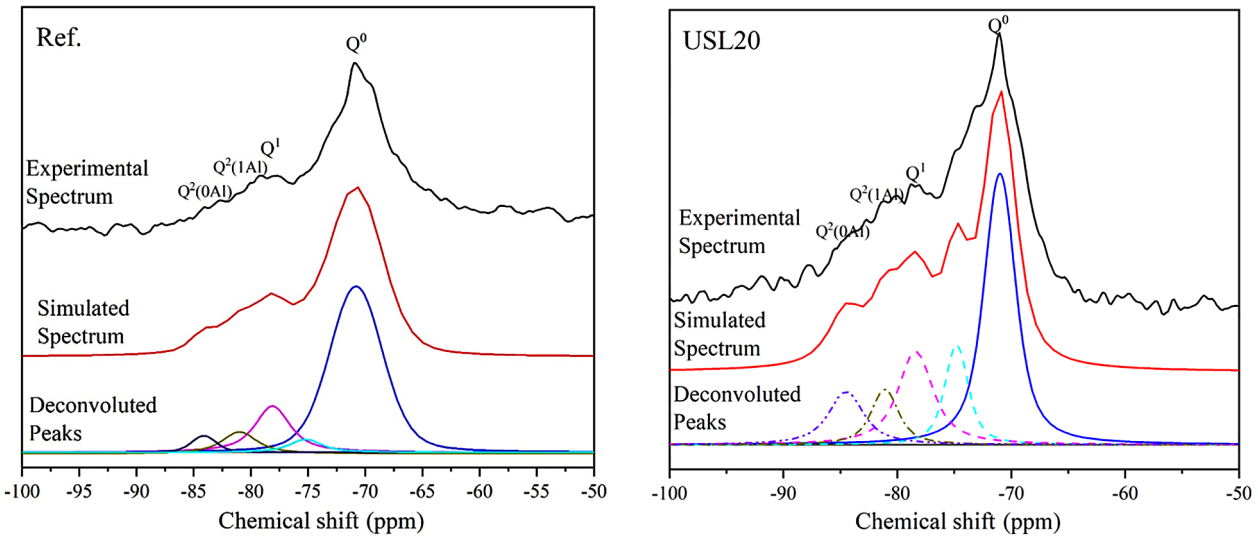

a) Ref. b) USL20

Figure 6. ^{29}Si NMR spectrums of UHPC.

Table 3. Deconvolution results for the ^{29}Si NMR spectra (%).

NO.		Q^0	Q^1	$Q^2(1Al)$	$Q^2(0Al)$	Al/Si	MCL
Ref	Peak (ppm)	–70.8	–78.1	–81.0	–84.1	0.107	3.25
	Area (%)	67.18	21.53	6.79	3.31	0.107	3.25
USL20	Peak (ppm)	–71.0	–78.4	–81.1	–84.5	0.235	4.46
	Area (%)	60.46	19.68	8.67	11.18	0.235	4.46

moved with different levels [20]. This demonstrated that the USL influenced the hydration of the cement paste and was involved in the hydration process. The mean chain length (MCL) and Al/Si of the C–S–H gels were calculated to better discriminate the effect of the USL on the hydration of the paste with Equations 2 and 3:

$$\text{Al/Si} = \frac{1/2\, Q^2\,(1\,\text{Al})}{Q^1 + Q^2\,(0\,\text{Al}) + Q^2\,(1\,\text{Al})} \tag{2}$$

$$\text{M Cl} = \frac{2\,[Q^1 + Q^2\,(0\,\text{Al}) + 3/2\, Q^2\,(1\,\text{Al})]}{Q^1} \tag{3}$$

where the Q^n represents the relative area after deconvolution. MCL and Al/Si are important parameters to characterise the degree of C–S–H polymerisation, the longer chain length indicated the higher degree of hydration [21]. Herein, MCL can be used as an indicator of the degree of hydration. The $Q^2(1Al)$ site indicated that Al was inserted into the C–S–H chain space and replaced the Si. The greater the relative area of $Q^2(1Al)$, the greater the substitution of Si in the C–S–H gel [22, 23]. The greater the relative area of $Q^2(1Al)$, the greater the substitution of A in the C–S–H gel [22, 23]. The relative area of $Q^2(1Al)$ in USL20 was 8.67 %, higher than the 6.79 % in the Ref. Similarly, the Al/Si increased from 0.107 to 0.235. The insertion of the element Al partially converted the C–S–H into C–(A)–S–H, which exhibited high polymerisation. Many studies have reported that the long MCL of C–S–H commonly facilitated the improvement of the compressive strength of cement-based materials [24, 25]. The same pattern was shown in this paper, which illustrated that the USL increased the polymerisation of C–S–H and enhanced the compressive strength.

MIP analysis

Figure 7 and Table 4 show the MIP results and pore structure characteristic parameters for Ref and USL20. After curing for 28 d, the porosity of USL20 containing 20 % USL was 6.72 %, which was a 14 % reduction compared to the Ref. From the pore size distribution diagram, it can also be found that most of the available pores will move to the left, indicating that the USL refined the pore structure [8]. The comparison of the

Table 4. Pore distribution of the UHPC.

Samples	Average pore diameter (nm)	Median pore diameter (nm)		Porosity (%)	Pore distribution (%)		
		by area method	by volume method	by volume	< 10 nm	10-100 nm	< 100 nm
USL20	18.58	18.73	16.76	6.72	7.76	67.64	24.6
Ref	20.16	19.63	17.76	7.83	5.52	63.68	29.8

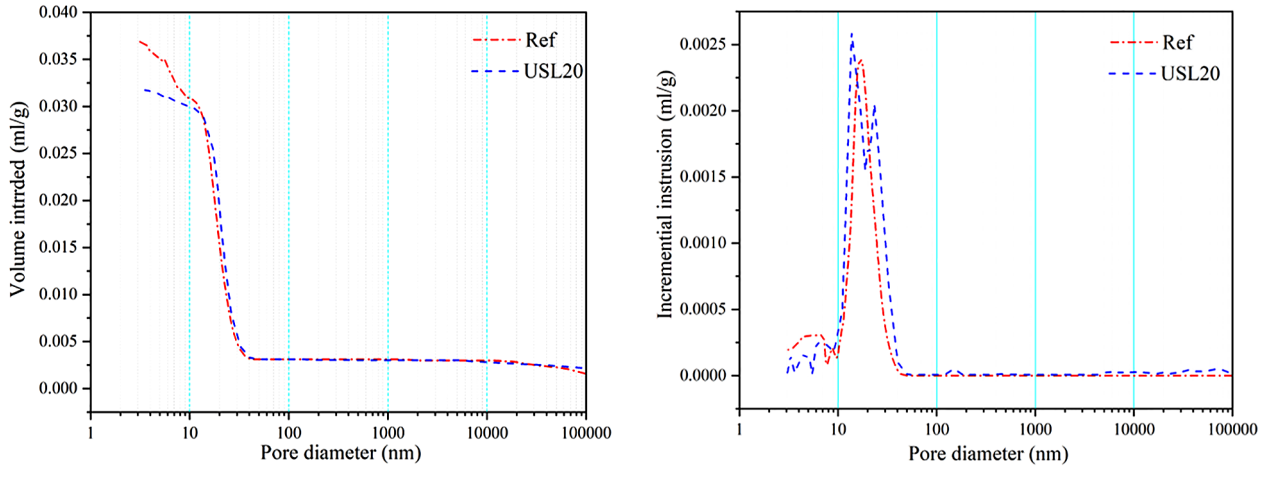

a) Ref. b) USL20

Figure 7. MIP results of Ref and USL20 at 28 days.

characteristic parameters of the pore structure in Table 4 revealed that the proportion of > 100 nm pores decreased after incorporating 20 % USL. Compared to the reference sample, the corresponding proportion of the pore sizes of < 10 nm and 10-100 nm in USL20 increased by 6.2 % and 40.5 %, respectively. The proportion of gel pores with a diameter of less than 10 nm increased significantly. Because the USL reacted with $Ca(OH)_2$ and produced the new C–S–H gel, which filled the large pores, it reduced the porosity and increased the density of the microstructure. This also explained why the addition of 20 % USL increased the compressive strength.

SEM analysis

The SEM images of Ref and USL20 at 1 d, 3 d, and 28 d are shown in Figure 8. Ref has a few pores, and the microstructure was relatively dense at 1 d. When incorporating 20 % USL, the pores in the paste increased, and the structure became loose, illustrating that the bond between the mineral powder particles and the slurry was unstable. However, compared to 1 d, USL20 obtained a denser microstructure at 7 d. The formation of flocculent C–S–H and other hydration products gradually filled in the middle of the USL and cement particles, making them more tightly bonded. After 28 d of hydration, the microstructure of Ref and USL20 was very dense with few visible pores, and plenty of hydration products were observed. Comparing the two figures, it can be found that the USL particles were covered by a large number of hydration products, which resulted in the connection between the mineral powder particles and the slurry becoming denser. There were two reasons for this [26, 27], one is that the size of USL particles was smaller than that of cement particles, which filled the pores between the cement particles, leading to a decrease in the porosity of the paste; secondly, large amounts of amorphous silica oxides and aluminium oxides dissolved from the USL reacted with $Ca(OH)_2$, the hydration product of cement and formed C–S–H and C-A-H gels in the UHPC high alkali environment, whose pozzolanic alkali-activated reaction enhanced the compactness of the paste which are also consistent with the NMR and MIP results. When incorporating 20% USL in the paste, the USL exhibited an excellent pozzolanic effect and filling effect. The synergistic effect of both significantly improved the degree of compactness of the paste and improved the mechanical properties of the UHPC.

BSE analysis

Figure 9 compares the BSE images of Ref and USL20 at 28 days. The brighter parts of the image are the unhydrated cement particles, the fragmented and smaller particles with darker colours are the USL particles, the black dots are pores within the paste and the other areas are C–S–H gels and other hydration products. A comparison of Figures 9a and 9b shows that the paste contained a small number of pores and a large number of unhydrated cement particles. Figure 9b further illustrated the filling effect of the USL promoted the homogenisation of the paste and improved the uniform distribution of the USL particles in the UHPC. Further magnification of the BSE microscopy image of the pastes revealed that the USL particles were covered by the hydration products in Figure 9b, indicating that secondary hydration of the USL particles occurred and organically combined with the surrounding hydration products [28].

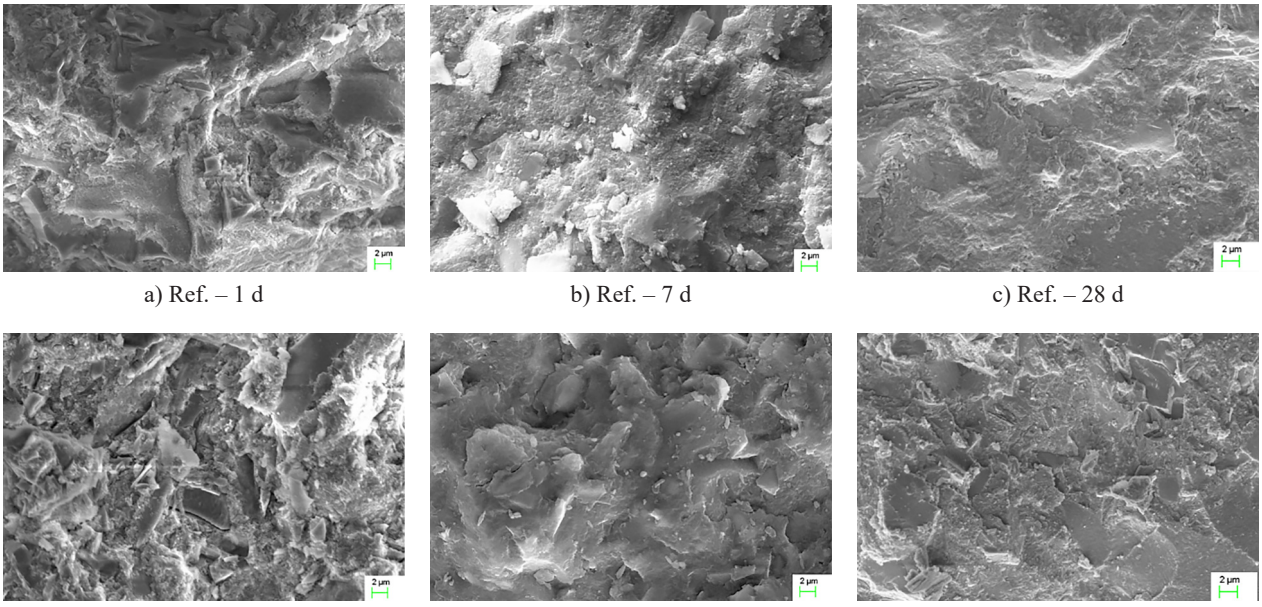

a) Ref. – 1 d b) Ref. – 7 d c) Ref. – 28 d

d) USL20 – 1 d e) USL20 – 7 d f) USL20 – 28 d

Figure 8. SEM images of Ref and USL20 at 1, 3, and 28 days.

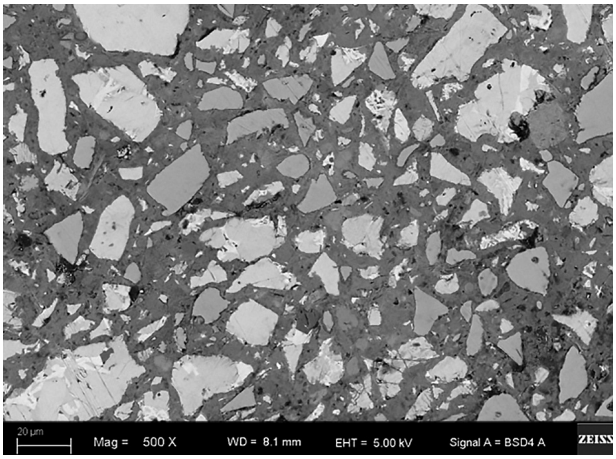

a) Ref. – 28 d

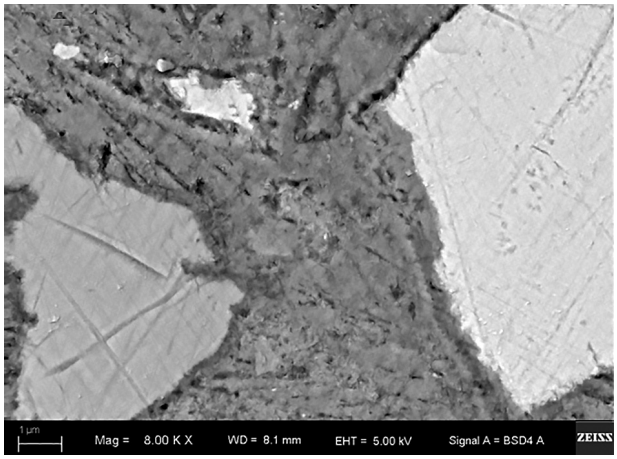

b) Ref. – 28 d

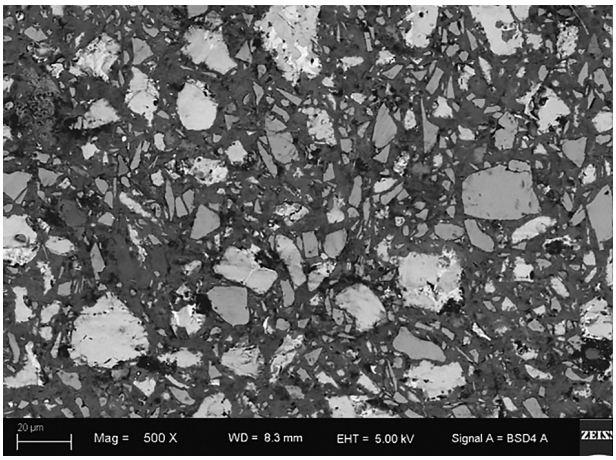

c) USL20 – 28 d

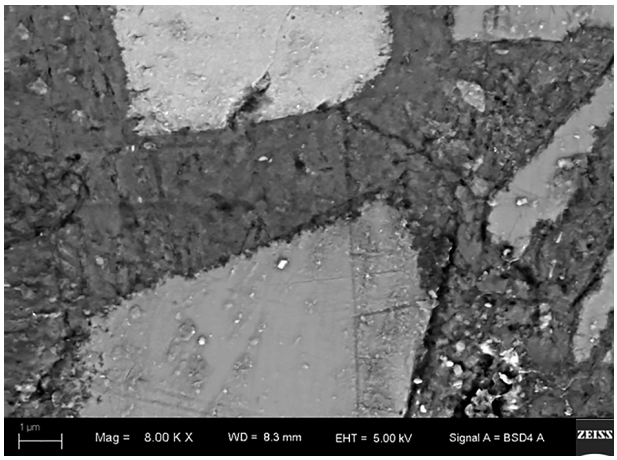

d) USL20 – 28 d

Figure 9. BSE image of the UHPC paste at 28 days.

This is further evidence that the addition of 20% USL improved the homogeneity of the microstructure of the hydration products and increased the denseness of the cement paste, which is consistent with the results presented by the MIP and SEM analyses.

XPS analysis

To deeply characterise the effect of the USL on the microstructure of the UHPC, Ca2p, Si2p and Al2p were chosen as the main atoms for the XPS analysis, the results of which are shown in Figure 10 and Table 5. After continuous hydration for 28–d, the binding energy of Ca2p, Si2p, and Al2p declined and shifted at a high frequency incorporating the 20 % USL. The binding energies shifted by 0.17 eV, 0.52 eV, 0.53 eV and 0.53 eV from the original peak binding energies of 346.62 eV, 100.93 eV, 530.83 eV and 73.59 eV for Ca2p, Si2p, O1s and Al2p, respectively. The Ca2p-Si2p value of USL20 was 245.34eV which is less than the 245.69 eV of the Ref, thus indicating that the USL increased the polymerisation of C–(A)–S–H and improved the binding energy at 28 days [29, 30]. In addition, the addition of USL reduced the Ca/Si ratio and increased the Al/Si ratio, which indicated that the pozzolanic reaction of USL occurred in the high alkali environment of the UHPC. Moreover, the Ca, Al, and Si elements were dissolved and more amorphous silicon oxides and alumina participated in the secondary hydration process, increasing the C–S–H polymerisation and the density of paste, which is consistent with the NMR results.

Table 5. Atomic parameters and binding energy of Ref and USL20 at 28 days.

	Peak binding energy(eV)				Ca2p-Si2p(eV)	Atomic (%)			
	O1s	Ca2p	Si2p	Al2p		O1s	Ca2p	Si2p	Al2p
Ref	530.83	346.62	100.93	73.59	245.69	53.09	11.71	4.02	3.81
USL20	531.36	346.79	101.45	73.88	245.34	47.21	9.53	4.23	4.01

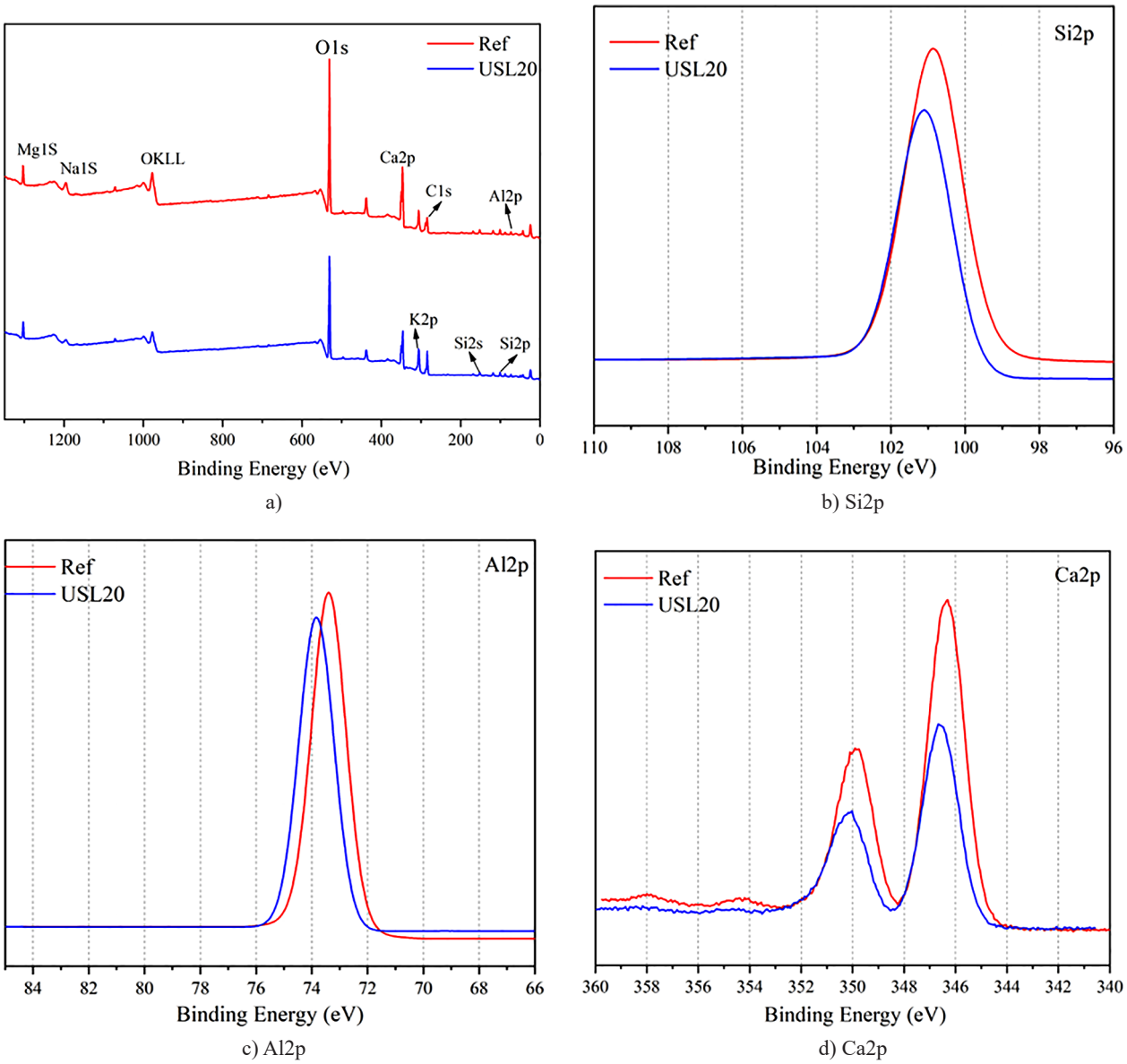

Figure 10. XPS spectra of Ref and USL20 with the main atoms of Ca2p, Si2p, and Al2p.

CONCLUSIONS

- The addition of USL unchanged the fluid type of the paste, which was still shear-thickened, but the yield stress showed a tendency to increase and then decrease with an increase in USL. The effect on the rheological behaviour index *n* was not significant.
- Incorporating 20 % ultrafine mineral powder, USL20 reached the maximum compressive strength of 147.8 MPa, which was increased by 12.2 % compared to the Ref, and its porosity was 6.72 %, which was decreased by 14 % compared to the Ref.
- Due to the pozzolanic reaction of USL, the chain length of C–S–H and the binding energy of Ca2p, Si2p, O1s, and Al2p increased, and the Al/Si ratio and Ca2P-Si2P value were reduced, leading to the microstructure of the paste being more compact.

Acknowledgments:

This research work was made possible thanks to financing from the National Natural Science Foundation of China (51872120), National Key R&D Program of China (No.2017YFB0309905), Natural Science Foundation of China (52002144), Natural Science Foundation of Shandong Province (ZR2020QE046).

REFERENCES

1. Bahmani H., Mostofinejad D. (2022): Microstructure of ultra-high-performance concrete (UHPC) – a review study. *Journal of Building Engineering*, *50*, 104118. Doi: 10.1016/j.jobe.2022.104118
2. Shah H. A., Yuan Q., Photwichai N. (2022): Use of materials to lower the cost of ultra-high-performance concrete – A review. *Construction and Building Materials*, *327*, 127045. Doi: 10.1016/j.conbuildmat.2022.127045

3. Luan C., Yang Q., Lin X., Gao X., Cheng H., Huang Y., et al. (2023): The Synergistic Effects of Ultrafine Slag Powder and Limestone on the Rheology Behavior, Microstructure, and Fractal Features of Ultra-High Performance Concrete (UHPC). *Materials*, *16*(6), 2281. Doi: 10.3390/ma16062281
4. Wang L., Yu Z., Liu B., Zhao F., Tang S., Jin M. (2022): Effects of fly ash dosage on shrinkage, crack resistance and fractal characteristics of face slab concrete. *Fractal and Fractional*, *6*(6), 335. Doi: 10.3390/fractalfract6060335
5. Yalçınkaya Ç., Çopuroğlu O. (2021): Hydration heat, strength and microstructure characteristics of UHPC containing blast furnace slag. *Journal of Building Engineering*, *34*, 101915. Doi: 10.1016/j.jobe.2020.101915
6. Ting L., Qiang W., Shiyu Z. (2019): Effects of ultra-fine ground granulated blast-furnace slag on initial setting time, fluidity and rheological properties of cement pastes. *Powder Technology*, *345*, 54-63. Doi: 10.1016/j.powtec.2018.12.094
7. Luan C., Wang J., Gao J., Wang J., Du P., Zhou Z., et al. (2022): Changes in fractal dimension and durability of ultra-high performance concrete (UHPC) with silica fume content. *Archives of Civil and Mechanical Engineering*, *22*(3), 123. Doi: 10.1007/s43452-022-00443-3
8. Shi C., Wang D., Wu L., Wu Z. (2015): The hydration and microstructure of ultra high-strength concrete with cement–silica fume–slag binder. *Cement and Concrete Composites*, *61*, 44-52. Doi:10.1016/j.cemconcomp.2015.04.013
9. Shirdam R., Amini M., Bakhshi N. (2019): Investigating the effects of copper slag and silica fume on durability, strength, and workability of concrete. *International Journal of Environmental Research*, *13*, 909-924. Doi: 10.1007/s41742-019-00215-7
10. Sharmila P., Dhinakaran G. (2016): Compressive strength, porosity and sorptivity of ultra fine slag based high strength concrete. *Construction and Building Materials*, *120*, 48-53. Doi: 10.1016/j.conbuildmat.2016.05.090
11. Zhou Y., Zhang Z. (2021): The hydration properties of ultra-fine ground granulated blast-furnace slag cement with a low water-to-binder ratio. *Journal of Thermal Analysis and Calorimetry*, *146*(4), 1593-1601. Doi: 10.1007/s10973-020-10181-4
12. Shanmugasundaram A., Jayakumar K. (2022): Effect of curing regimes on microstructural and strength characteristics of UHPC with ultra-fine fly ash and ultra-fine slag as a replacement for silica fume. *Arabian Journal of Geosciences*, *15*(4), 345. Doi: 10.1007/s12517-022-09617-y
13. Zhu Z., Chen H., Liu L., Li X. (2017): Multi-scale modelling for diffusivity based on practical estimation of interfacial properties in cementitious materials. *Powder Technology*, *307*, 109-118. Doi: 10.1016/j.powtec.2016.11.036
14. Zhu Z., Provis J. L., Chen H. (2018): Quantification of the influences of aggregate shape and sampling method on the overestimation of ITZ thickness in cementitious materials. *Powder Technology*, *326*, 168-180. Doi: 10.1016/j.powtec.2017.12.008
15. Wang L., Luo R., Zhang W., Jin M., Tang S. (2021): Effects of fineness and content of phosphorus slag on cement hydration, permeability, pore structure and fractal dimension of concrete. *Fractals*, *29*(02), 2140004. Doi: 10.1142/s0218348x21400041
16. Zhu J., Xie W., Li Z., Liu J., Ran Q., Li X., et al. (2022): An approach to describe the shear-thickening viscosity of cement paste incorporating microfines of manufactured sand. *Construction and Building Materials*, *340*, 127743. Doi: 10.1016/j.conbuildmat.2022.127743
17. Mo L., Liu M., Al-Tabbaa A., Deng M., Lau W. Y. (2015): Deformation and mechanical properties of quaternary blended cements containing ground granulated blast furnace slag, fly ash and magnesia. *Cement and Concrete Research*, *71*, 7-13. Doi: 10.1016/j.cemconres.2015.01.018
18. Li H., Farzadnia N., Shi C. (2018): The role of seawater in interaction of slag and silica fume with cement in low water-to-binder ratio pastes at the early age of hydration. *Construction and Building Materials*, *185*, 508-518. Doi: 10.1016/j.conbuildmat.2018.07.091
19. Luan C., Zhou Y., Liu Y., Ren Z., Wang J., Yuan L., et al. (2022): Effects of nano-SiO_2, nano-$CaCO_3$ and nano-TiO_2 on properties and microstructure of the high content calcium silicate phase cement (HCSC). *Construction and Building Materials*, *314*, 125377. Doi: 10.1016/j.conbuildmat.2021.125377
20. Wang L., Guo F., Lin Y., Yang H., Tang S. W. (2020): Comparison between the effects of phosphorous slag and fly ash on the CSH structure, long-term hydration heat and volume deformation of cement-based materials. *Construction and Building Materials*, *250*, 118807. Doi: 10.1016/j.conbuildmat.2020.118807
21. Wang L., Jin M., Zhou S., Tang S., Lu X. (2021): Investigation of microstructure of CSH and micro-mechanics of cement pastes under NH_4NO_3 dissolution by ^{29}Si MAS NMR and microhardness. *Measurement*, *185*, 110019. Doi: 10.1016/j.measurement.2021.110019
22. Li J., Liu X., Yang Q., Hou D., Hu X., Ye Q., et al. (2020): Characterization of fly ash-cement paste and molecular structure in the presence of seawater by ^{27}Al and ^{29}Si MAS NMR spectroscopy. *Construction and Building Materials*, *262*, 120823. Doi: 10.1016/j.conbuildmat.2020.120823
23. Zou F., Hu C., Wang F., Ruan Y., Hu S. (2020): Enhancement of early-age strength of the high content fly ash blended cement paste by sodium sulfate and C–S–H seeds towards a greener binder. *Journal of Cleaner Production*, *244*, 118566. Doi: 10.1016/j.jclepro.2019.118566
24. Chen Y. L., Lin C. J., Ko M. S., Lai Y. C., Chang J. E. (2011): Characterization of mortars from belite-rich clinkers produced from inorganic wastes. *Cement and Concrete Composites*, *33*(2), 261-266. Doi: 10.1016/j.cemconcomp.2010.10.012
25. Wu D. S., Peng Y. N. (2003): The macro-and micro properties of cement pastes with silica-rich materials cured by wet-mixed steaming injection. *Cement and Concrete Research*, *33*(9), 1331-1345. Doi: 10.1016/s0008-8846(03)00059-0
26. Lal C. M., Sai Srujan Reddy V. (2017): Properties of High Strength Fibre Reinforced Concrete Using Ultra Fine Slag. In *Applied Mechanics and Materials* (Vol. 857, pp. 183-188). Trans Tech Publications Ltd. Doi: 10.4028/www.scientific.net/AMM.857.183
27. Teng S., Lim T. Y. D., Divsholi B. S. (2013): Durability and mechanical properties of high strength concrete incorporating ultra fine ground granulated blast-furnace slag. *Construction and Building Materials*, *40*, 875-881. Doi: 10.1016/j.conbuildmat.2012.11.052
28. Li W., Yi L., Jiang W., Dong H., Zhang Y. (2022): Effects of Ultrafine Blast Furnace Slag on the Microstructure and Chloride Transport in Cementitious Systems under Cyclic Drying–Wetting Conditions. *Applied Sciences*, *12*(8), 4064. Doi: 10.3390/app12084064
29. Kurumisawa K., Nawa T., Owada H., Shibata M. (2013): Deteriorated hardened cement paste structure analyzed by XPS and 29Si NMR techniques. *Cement and Concrete Research*, *52*, 190-195. Doi: 10.1016/j.cemconres.2013.07.003
30. Bykov G. L., Abkhalimov E. V., Ershov V. A., Ershov B. G. (2021): Effect of gamma irradiation on Portland cement: Hydrogen evolution and radiation resistance. *Construction and Building Materials*, *295*, 123644. Doi: 10.1016/j.conbuildmat.2021.123644